Research Square

Preprints are preliminary reports that have not undergone peer review.
They should not be considered conclusive, used to inform clinical practice,
or referenced by the media as validated information.

Temporal Changes in Plasma Metabolites After Initial Beetroot Powder Intake and During Continued Supplementation: A Targeted Metabolomics Study

Wenjing Guo
Capital University of Physical Education and Sports
Zepeng Hu
Shanghai University of Sport
Tieying Li
National Institute of Sports Medicine
Nan An
National Institute of Sports Medicine
Hao Wu
shoudutiyuan1@163.com

Capital University of Physical Education and Sports

Research Article

Keywords: beetroot powder, targeted metabolomics, linear mixed-effects model, dimethylglycine, fatty acids

Posted Date: November 24th, 2026

DOI: https://doi.org/10.21203/rs.3.rs-11723211/v1

License: This work is licensed under a Creative Commons Attribution 4.0 International License.
Read Full License

Additional Declarations: No competing interests reported.

Temporal Changes in Plasma Metabolites After Initial Beetroot Powder Intake and During Continued Supplementation: A Targeted Metabolomics Study

Wenjing Guo[1] †, Zepeng Hu[2]†, Tieying Li[3], Nan An[3]*, Hao Wu[1] *

Affiliations:

[1] School of Sport Science and Health, Capital University of Physical Education and Sports, Beijing 100191, China

[2] School of Exercise and Health, Shanghai University of Sport, Shanghai 200438, China

[3] Sports Nutrition Center, National Institute of Sports Medicine, Beijing 100029, China

Email: 17765118586@163.com (Wenjing Guo)

Email: huzepeng2019@cupes.edu.cn (Zepeng Hu)

Email: ltieying@163.com (Tieying Li)

† These authors contributed equally to this work.

*Corresponding authors:

Hao Wu

Tel: +86-18435224613

Email: shoudutiyuan1@163.com

Nan An

Email: annan@sports-nutrition.org.cn

Temporal Changes in Plasma Metabolites After Initial Beetroot Powder Intake and During Continued Supplementation: A Targeted Metabolomics Study

Abstract

Background/Objectives: To characterize plasma metabolite changes over 24 h after initial beetroot powder intake and after continued supplementation in healthy young men.

Methods: In a single-group longitudinal study, 24 participants consumed 40 g of beetroot powder daily for 14 d. Blood was collected before and 0.5–24 h after initial intake and after an overnight fast on the mornings following the seventh and fourteenth doses. Linear mixed-effects models assessed 201 metabolites in 214 samples. Overall time-effect tests and planned baseline contrasts were separately adjusted using the Benjamini–Hochberg procedure ($q < 0.05$). Trajectory clustering and over-representation analyses were performed.

Results: Overall time effects were significant for 155 metabolites; 128 differed from baseline at one or more time points. Significant changes were predominantly decreases at 0.5–2 h and increases at 6–12 h, with 99 and 81 responsive metabolites at 6 and 12 h, respectively. Four temporal patterns were identified. The early-decrease cluster comprised mainly fatty acids and related lipids (12/13); linoleic acid metabolism was the only significantly enriched human KEGG pathway ($q = 0.0143$). Only dimethylglycine remained significantly elevated at the fasting assessment following the fourteenth dose.

Conclusions: Plasma metabolic responses showed temporal and molecular heterogeneity. Early fatty acid decreases and later fasting dimethylglycine elevation identify candidate features for controlled validation. Without a concurrent control, these changes cannot be attributed solely to beetroot powder.

Keywords: beetroot powder; targeted metabolomics; linear mixed-effects model; dimethylglycine; fatty acids

1 Introduction

Beetroot (*Beta vulgaris* L.) products have attracted considerable attention because they are rich in dietary nitrate. Webb et al. found that beetroot juice intake in healthy participants increased plasma nitrite and was accompanied by lower blood pressure, attenuated ischemia–reperfusion-induced endothelial dysfunction, and reduced platelet aggregation measured ex vivo [1]. Larsen et al. observed improved mitochondrial oxidative phosphorylation efficiency in human skeletal muscle in a trial of inorganic nitrate supplementation [2]. These studies have made the nitrate–nitrite–nitric oxide pathway a central focus of human beetroot research. However, vascular function, tissue

energy metabolism, and circulating metabolite profiles provide information at different levels; physiological and tissue-level evidence cannot substitute for direct measurement of the plasma metabolome.

In addition to nitrate, beetroot products contain multiple components that may contribute to circulating metabolic responses. The content of a component in food does not equate to plasma exposure to that component or its metabolites. Comparing beetroot juice with whole beetroot, Clifford et al. found that both products increased total plasma nitrate and nitrite (NOx), whereas betanin detected in both products was not detected in plasma at the designated sampling times 1–8 h after intake [3]. In a randomized crossover trial with equal nitrate intake, Jurga et al. observed increases in plasma betaine and choline after beetroot juice intake, reaching their highest levels among the study's designated sampling times at 1 h [4]. Thus, neither product composition alone nor a few nitrate-related markers can adequately capture the circulating metabolic changes that actually occur after intake.

Sampling time also affects the interpretation of metabolic responses. During 24 h of observation after different doses of beetroot juice, Wylie et al. found dose- and time-dependent changes in plasma nitrate and nitrite [5]; the betaine and choline changes observed by Jurga et al. occurred mainly at earlier sampling times [4]. In a study of continued supplementation, Miller et al. measured plasma nitrate and nitrite both in the fasting state and after intake on the same day, and observed changes in fasting levels relative to baseline during continued supplementation [6]. Moreover, standardized meals can themselves alter the temporal trajectories of amino acids and one-carbon metabolism-related molecules; post-intake plasma changes must therefore be interpreted in the context of meal and blood-sampling schedules [7]. These studies suggest that dense temporal observation after the initial intake and fasting measurements after continued supplementation provide complementary information. Observing only one time point after the initial intake may miss transient changes and cannot assess differences between the morning fasting state after continued supplementation and the initial baseline.

Metabolomics has begun to be used to examine human responses to beetroot products. Kozłowska et al. analyzed the urinary metabolome of fencers at the end of an exercise test following continued supplementation [8], and Stander et al. examined serum metabolic changes during beetroot juice supplementation after a marathon [9]. Another study included observations after both a single intake and continued supplementation, but mainly measured nitric oxide-related, oxidative stress, and inflammatory markers [10]. These studies have broadened understanding of human metabolic responses to beetroot products, but were largely conducted in the context of exercise or focused on urinary or serum metabolomes or a small number of prespecified markers. Multitime-point plasma changes after initial beetroot powder intake, and their

relationship with fasting metabolic features after continued supplementation, remain to be further described.

Accordingly, this study used a single-group longitudinal repeated-measures design in healthy young men to examine plasma metabolite changes by targeted metabolomics during the 24 h after initial beetroot powder intake and in the fasting state on the mornings after the seventh and fourteenth doses. The study aimed to describe temporal responses of the overall metabolic profile and individual metabolites relative to the initial baseline, characterize response patterns shared across and differing between sampling times, and explore the metabolite composition of distinct temporal patterns, thereby informing the selection of target molecules and sampling times for subsequent controlled studies.

2 Materials and Methods

This study used a single-group within-participant before-and-after repeated-measures design without a placebo control or blinding. It was conducted at the Comprehensive Key Laboratory for Sports Performance Evaluation and Research of the General Administration of Sport of China. The study was approved by the Ethics Committee of Capital University of Physical Education and Sports (approval no. 2025A162) and adhered to the Declaration of Helsinki. All participants voluntarily provided written informed consent after being informed of the study purpose, procedures, and potential risks.

2.1 Study Design and Participants

Twenty-four healthy male university students were recruited. Their age, baseline height, weight, and body mass index (BMI) were 20.25 ± 0.94 years, 179.60 ± 7.22 cm, 74.80 ± 13.13 kg, and 23.16 ± 3.70 kg/m², respectively. Participants were recruited from a single class comprising predominantly male students. For practical feasibility, only men were enrolled. The inclusion criteria were as follows:

(1) Age 18–25 years and participation in at least 150 min of moderate-intensity exercise per week, verified by questionnaire;

(2) No history of cardiovascular, hepatic, renal, gastrointestinal, or endocrine-metabolic disease; no major musculoskeletal injury or other chronic systemic disease; and no history of cardiovascular medication use, as determined by a medical questionnaire;

(3) A response of “no” to every item of the Physical Activity Readiness Questionnaire (PAR-Q);

(4) No smoking habit or alcohol dependence, and no use of antibiotics, anti-inflammatory drugs, or other drugs or nutritional supplements that might affect redox metabolism or exercise capacity within 3 months before screening;

(5) Not a long-term vegetarian and no habitual high consumption of nitrate-rich foods such as spinach, celery, arugula, or beetroot products;

(6) Ability to complete the study procedures on schedule and comply with dietary restrictions and supplement intake recording requirements.

This metabolomics analysis used plasma samples collected under the study protocol described above. No prospective sample-size calculation was performed for the metabolomics outcomes; the analyses were therefore considered exploratory.

2.2 Beetroot Powder Supplementation Protocol

Participants consumed 40 g of beetroot powder mixed with 350 mL of drinking water once daily at a fixed morning time for 14 days. The powder was provided in individually packaged doses from a single batch. According to the batch certificate of analysis, the nitrate content was 17.3 mg/g, corresponding to approximately 692 mg (11.2 mmol) of nitrate per dose; nitrate content was not independently measured in this study. The first intake was designated as the first dose on Day 1.

2.3 Blood-Sampling Time Points and Observation

On the day of the initial dose, a baseline blood sample was collected at 08:30 after an overnight fast and designated 0 h (H0). Participants then immediately consumed the beetroot powder drink. Time was measured from completion of the drink, and blood was collected 0.5, 1, 2, 6, 12, and 24 h after intake, designated H0.5, H1, H2, H6, H12, and H24. The scheduled clock times were approximately 09:00, 09:30, 10:30, 14:30, 20:30, and 08:30 the following morning; elapsed time after intake was calculated from completion of the drink. The H24 sample was collected in the fasting state the following morning before that day's dose. On the mornings after the seventh and fourteenth doses, that is, at approximately 08:30 on Days 8 and 15, fasting D7 and D14 samples were collected, respectively; the D7 sample was collected before the eighth dose.

After the initial intake, breakfast, lunch, and dinner were provided at 09:35, 13:30, and 17:30, respectively, between the H1 and H2, H2 and H6, and H6 and H12 blood draws. H0–H24 was used to describe acute changes after the initial intake, whereas D7 and D14 were used to describe next-morning fasting changes after continued supplementation. The study design and sampling procedure are shown in

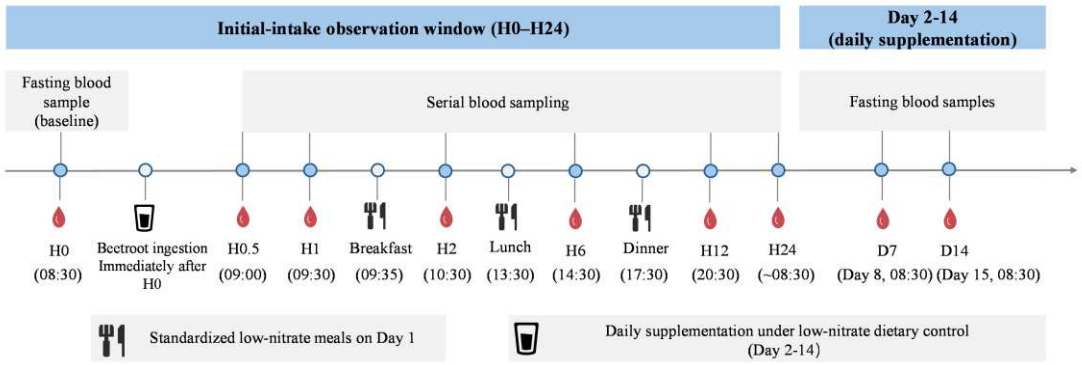

Fig. 1.

2.4 Blood Sample Collection and Storage

Trained nurses collected blood from an antecubital vein into ethylenediaminetetraacetic acid (EDTA) anticoagulant tubes. Immediately after collection, samples were centrifuged at 4 °C and 3000 × g for 10 min to separate plasma. The upper plasma layer was then aspirated, aliquoted into 1.5 mL cryovials, and stored at −80 °C until metabolomic analysis. All samples underwent the same processing procedure.

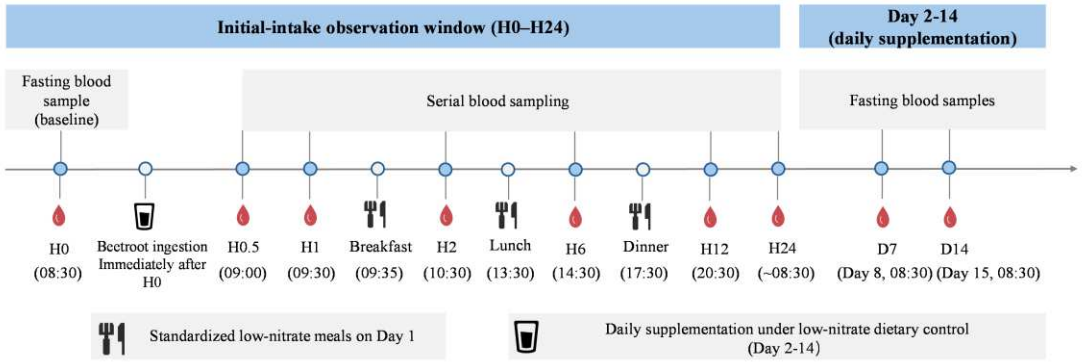

Fig. 1 Study design and serial blood-sampling schedule during 14 days of beetroot powder supplementation.

Standardized low-nitrate meals were provided during the acute 0–24-h assessment, and low-nitrate dietary control was maintained during Days 2–14. D7 and D14 denote fasting blood samples collected on the mornings of Days 8 and 15, respectively. The timeline is schematic and not drawn to scale.

2.5 Standardized Experimental Controls

(1) Supplementation and sampling schedule: All participants completed beetroot powder supplementation and blood collection according to a common schedule. Actual dosing and sampling times were recorded to reduce the influence of timing differences on metabolite concentrations. Before H0, H24, D7, and D14 blood collection, participants consumed no food or energy-containing beverages after finishing dinner the preceding evening; water was permitted, and blood was collected the following morning after an overnight fast.

(2) Mouthwash, diet, and supplement control: Participants stopped using antibacterial mouthwash 7 d before the formal experiment [11]. During the 14-d supplementation period, they followed a low-nitrate diet and avoided nitrate-rich vegetables, other beetroot products, processed meats containing nitrite preservatives, and tea, coffee, fruit juice, and alcoholic beverages. For 48 h before each sampling phase, they followed additional low-nitrate and low-polyphenol dietary restrictions and were prohibited from using additional nutritional supplements that might affect redox status or nitric oxide metabolism. To monitor adherence to dietary control, participants reported each meal daily through the study's WeChat group. Researchers sent daily dietary reminders in the group and reviewed the reports. All actual sampling times were entered on a standardized record form.

(3) Diet during the acute phase: Breakfast consisted of shrimp, mushrooms, and pumpkin; lunch consisted of eggs, chicken, shrimp, and rice; and dinner consisted of chicken, potatoes, fish, and rice. Ingredients, portion sizes, and cooking methods were kept consistent, and nitrate-rich foods were avoided.

2.6 Targeted Metabolomics Analysis

Plasma samples were analyzed using the HM Meta high-throughput targeted metabolomics platform. Target metabolite signals were acquired using an ACQUITY UPLC I-Class ultra-performance liquid chromatography (UPLC) system (Waters, USA) coupled to a QTRAP 6500 Plus mass spectrometry system in electrospray ionization (ESI) and multiple reaction monitoring (MRM) modes. Reported names were based on platform-prespecified ion transitions, retention times, and related information. Configurations or isomers for which sufficient discriminatory evidence was unavailable were not assigned structures beyond the capability of the analytical method.

2.6.1 Sample Extraction and Derivatization

Plasma samples and calibration standards were processed separately. To 20 μL of plasma or standard solution, 150 μL of sample release reagent containing internal standards was added. After shaking at 1200 rpm for 30 min, the mixture was centrifuged at 4 °C and 18 000 × g for 30 min. A 40-μL aliquot of supernatant was transferred to a 96-well plate, and 25 μL of derivatization reagent and 25 μL of 1-ethyl-3-(3-dimethylaminopropyl)carbodiimide (EDC) working solution were added. The mixture was incubated for 60 min at 40 °C with shaking at 1200 rpm, then centrifuged at 4 °C and 4000 × g for 5 min. After adding 90 μL of 50% aqueous methanol, it was mixed at 600 rpm for 10 min and centrifuged at 4 °C and 4000 × g for 30 min before instrumental analysis. Internal standards were matched by metabolite class or chemical structural similarity; a separate isotope-labeled internal standard was not available for every target metabolite.

2.6.2 Chromatographic and Mass Spectrometric Conditions

The column was a BEH C18 (2.1 mm × 100 mm, 1.7 μm; Waters) maintained at 40 °C. Mobile phase A was 0.1% aqueous formic acid, and mobile phase B was acetonitrile containing 30% isopropanol. The B-phase gradient over 0–1, 1–5, 5–9, 9–11, 11–13.5, 13.5–14, 14–16, and 16–18 min was 5%, 5%–30%, 30%–50%, 50%–78%, 78%–95%, 95%–100%, 100%, and 5%, respectively. The flow rate was 0.600 mL/min at 14–16 min and 0.400 mL/min during all other intervals.

The ion-source temperature was 500 °C, and spray voltages in positive and negative ion modes were 4500 V and −4500 V, respectively. The pressures of ion-source gases I and II and curtain gas were 60, 60, and 35 psi, respectively. The MRM method was set according to target precursor–product ion pairs, collision energies, declustering potentials, and retention times.

2.7 Metabolite Identification, Quantification, and Data Quality Control

Skyline (v21.1.0.146) was used to extract and integrate target MRM chromatographic peaks [12]. The platform used 11-point calibration curves: separate analyte-specific curves for nonlipid metabolites and class-specific curves for lipids. Concentrations were reported in μmol/L after correction using class-matched or structurally similar internal standards. The testing laboratory provided a quantification status for every result. Only values within the reliable quantification range were regarded as valid concentrations; results classified as not detected, below the lower limit of quantification (LLOQ), or above the upper limit of quantification (ULOQ) were treated as missing. Valid observation counts for each metabolite at each sampling time point and a summary of missing-data reasons are provided in Supplementary Table S2. A metabolite's invalid-result rate was defined as the proportion of results that were not detected, below the LLOQ, or above the ULOQ among the relevant study samples or quality control (QC) samples.

Formal quality evaluation used 13 QC samples of the same type and concentration level; the initial QC injections used for instrument equilibration were not included. Metabolites were required to satisfy all three criteria: an invalid-result rate ≤20% in study samples, an invalid-result rate ≤20% in QC samples, and a QC relative standard deviation (RSD) ≤30%. RSD was calculated using valid QC concentrations only. Analytical stability was also assessed using correlations among QC samples, clustering in principal component analysis (PCA), and the relationship between QC concentrations and injection order.

After metabolite screening, sample-level quality review was performed. Candidate anomalous samples were first identified from each study sample's invalid-result rate and exploratory PCA, and then reviewed using adjacent within-participant temporal trajectories, the principal driving metabolites, quantification statuses, analytical batch, and injection order. Samples were not automatically removed because of a single extreme concentration or PCA outlier position; exclusion required multiple lines of evidence supporting a technical anomaly.

All valid concentrations were $\log_2$-transformed. No additional normalization by sample total, quantile normalization, probabilistic quotient normalization, or QC-based injection-order correction was performed. The primary single-metabolite analyses used unimputed, unscaled $\log_2$ concentrations, with each model estimated from all available observations for the corresponding metabolite.

Missing values were imputed only for exploratory analyses requiring a complete matrix, such as PCA. Random masking and low-abundance-biased masking scenarios were constructed separately according to the actual number of missing values for each metabolite at each time point. Each scenario was repeated three times to compare recovery errors and the consistency of the resulting PCA structure for time-point median, k-nearest-neighbor, and iterative Extra Trees imputation. Based on the

validation results, iterative Extra Trees imputation was used to construct the exploratory complete matrix.

Metabolite names, abbreviations, Human Metabolome Database (HMDB) identifiers, Kyoto Encyclopedia of Genes and Genomes (KEGG) identifiers, and class information were reviewed against the testing platform's documentation and the final reportable names confirmed by the testing laboratory. The retained metabolites were assigned to 10 unified classes based on their annotations; class assignments were not changed according to temporal response results. For the human KEGG pathway analysis [13], mappings were established using reportable names, the structural level supported by the analytical method, and database entries. Metabolites whose names could reasonably correspond to a KEGG entry but whose stereochemical forms or isomers could not be further distinguished by the method were retained as candidate mappings and included in the primary analysis. A strict-mapping sensitivity analysis included only metabolites without clear identity or identifier disputes. Metabolites with an explicit name–identifier mismatch that could not be corrected, or for which differences among candidate structures could alter pathway assignment but could not be resolved, were excluded from pathway analysis; those passing quality screening remained in analyses independent of pathway annotation. Item-level annotations and unified classes are provided in Supplementary Table S1.

2.8 Statistical Analysis

Exploratory PCA used imputed $\log_2$ concentrations, with each metabolite mean-centered and scaled by its standard deviation (autoscaling) [14]. PCA was used to describe the major sources of variation and screen for candidate anomalous samples, not as a formal test of differences between time points.

For the primary longitudinal analysis, a random-intercept linear mixed-effects model (LMM) was fitted separately for each metabolite. Unimputed, unscaled $\log_2$ concentration was the dependent variable; nine-level sampling time was a categorical fixed effect; a random intercept was specified for each participant; and H0 was the reference. All time points from H0 to D14 were included in the same model. Restricted maximum likelihood estimation and a Satterthwaite degrees-of-freedom approximation were used to test the overall time effect [15, 16], and estimated marginal means were used to calculate the eight planned contrasts against H0. Models used all available observations after quality review and did not require each participant to complete all nine blood draws. Time-point contrasts were not contingent on a significant overall time effect. The estimate β was on the $\log_2$ scale; fold change (FC) was defined as $FC=2^{\beta}$, and 95% confidence intervals (CIs) were back-transformed in the same way.

The overall time effects (201 tests) and planned time-point contrasts ($201 \times 8 = 1{,}608$ tests) were treated as separate testing families for Benjamini–Hochberg false discovery rate (BH-FDR) correction, with $q<0.05$ used as the exploratory significance criterion. β, FC, 95% CIs, unadjusted P values, and q values were also reported, without

an additional FC screening threshold. Model diagnostics assessed convergence and singular fits, conditional residual distributions, and the relationship between residuals and fitted values. Leave-one-participant-out refitting was used to assess the sensitivity of effect estimates and significance after unified correction to individual participants. Diagnostic findings were not used to exclude samples automatically.

For metabolites with $q<0.05$ in at least one planned contrast, an UpSet plot summarized the exact intersections of significant time points. Based on the direction of the LMM β estimates at the corresponding significant time points, responses were described as consistently increased, consistently decreased, or bidirectional. The LMM β estimates for the eight nonbaseline time points relative to H0 were standardized to within-metabolite row Z scores, followed by hierarchical clustering using Euclidean distance and Ward.D2 linkage. Among candidate solutions with 2–8 clusters and a minimum cluster size of at least eight metabolites, the number of clusters with the highest mean silhouette coefficient was selected [17]. The class response rate was defined as the number of metabolites in a class with $q<0.05$ in at least one planned contrast divided by the total number of analyzed metabolites in that class. Class response rates and numbers of significant molecular species in the lysophosphatidylcholine (LPC), lysophosphatidylethanolamine (LPE), and phosphatidylethanolamine (PE) subclasses were summarized descriptively only, without formal statistical comparisons between classes or subclasses.

Using the 128 responsive metabolites as the primary background, each of the four temporal response clusters was used as a foreground set for one-sided Fisher's exact tests of over-representation in the 10 unified classes. BH-FDR correction was applied jointly to the 40 tests formed by four clusters × 10 classes. A sensitivity analysis used all 201 retained metabolites as the background. The primary human KEGG pathway analysis used 59 mappable metabolites as the background and included only 29 human metabolic pathways containing at least two metabolites from this background. One-sided Fisher's exact tests assessed pathway over-representation in each temporal response cluster, and BH-FDR correction was applied jointly to the 116 tests formed by four clusters × 29 pathways. Sensitivity analyses used 48 responsive and mappable metabolites and 53 strictly mapped metabolites as backgrounds. Disease, signaling, and plant- or microorganism-specific pathways were excluded. Pathway results were interpreted in light of mapping coverage, the background set, and the number of mappable metabolites in each cluster.

Betaine, dimethylglycine, sarcosine, and glycine were presented as candidate metabolic features relevant to the study background; citrulline, ornithine, and homoarginine were reported as secondary exploratory results. These presentations were based on the already defined overall time effects and planned time-point contrasts. They did not constitute new independent hypothesis tests and were not used to infer metabolic flux, pathway activation, or beetroot-specific causal effects.

Linear mixed-effects models, planned contrasts, and Figures 2–7 were generated using R (version 4.6.1), with the lme4, lmerTest, emmeans, ggplot2, and ComplexHeatmap packages. Data preparation, artificial masking validation, and preliminary exploratory analyses were performed using Python (version 3.12). One-sided Fisher's exact tests were used for class and pathway over-representation analyses; planned time-point contrasts used two-sided tests, and overall time effects used F tests.

3 Results

3.1 Data Quality Control and Final Analysis Set

The initial quantitative matrix contained 322 targeted metabolites, 215 study plasma samples, and 13 formal QC samples. Based on the prespecified criteria of invalid-result rates ≤20% in both study and QC samples and a QC relative standard deviation (RSD) ≤30%, 201 metabolites were retained. The median QC RSD of retained metabolites was 16.03% (interquartile range, 11.88%–20.99%). The median pairwise Spearman correlation among the 13 QC samples was 0.990 (minimum, 0.981). No statistically significant monotonic association was observed between the overall QC signal and injection order ($\rho=-0.181$, $P=0.553$).

The G5b sample at H6 was excluded because 52/201 metabolites (25.9%) were not reliably quantified and its within-participant trajectory and PCA position were anomalous. One additional H24 blood sample was not submitted for analysis because of hemolysis. The final analysis included 214 samples from 24 participants and 201 metabolites, with 23 samples each at H6 and H24 and 24 samples at each remaining time point. There were 1,019 missing results (2.37%) among the 201 metabolites in this matrix. The final retained metabolites and their annotations are listed in Supplementary Table S1.

3.2 Temporal Characteristics of the Overall Metabolite Profile

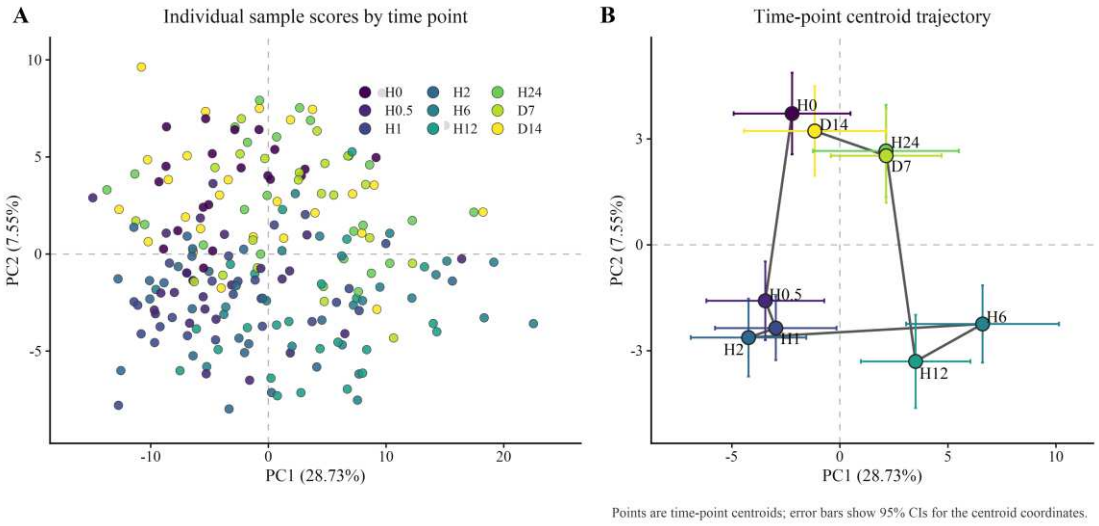

Fig. 2 Temporal trajectory of the overall plasma metabolite profile during beetroot powder supplementation

Valid concentrations of 201 metabolites were $\log_2$-transformed; missing values were imputed and autoscaling was applied only for PCA. A total of 214 study samples were analyzed. (A)

Individual sample PC1–PC2 scores at each time point. (B) Time-point centroids with 95% confidence intervals for each coordinate, calculated as the mean ± $t_{0.975,n-1}$ × standard error, where n is the number of samples at the corresponding time point. Connecting lines indicate the sampling sequence only. PC1 and PC2 explained 28.73% and 7.55% of total variation, respectively. One H6 sample was excluded after quality review, and one H24 blood sample was not submitted for analysis because of hemolysis; these time points therefore each had 23 samples, whereas all others had 24. PCA was used for exploratory description only, not for formal testing of time-point differences.

In exploratory PCA of 201 metabolites and 214 samples, PC1 and PC2 explained 28.73% and 7.55% of total variation, respectively (Fig. 2A), or 36.28% combined. Individual samples overlapped extensively across time points and did not form clearly separated time-point clusters; however, time-point centroids showed stage-dependent shifts in the PC1–PC2 plane. Relative to H0, H0.5–H2 moved mainly in the negative PC2 direction, while H6–H12 shifted further in the positive PC1 direction. H24 and D7 occupied a transitional region, and D14 again approached H0 in the first two principal-component dimensions (Fig. 2B). These findings suggest a time-related pattern of stage-dependent shifts in the plasma metabolite profile in the first two principal-component dimensions during the study. Specific time effects and their significance were evaluated using the subsequent linear mixed-effects models.

3.3 Time-Dependent Metabolic Changes Identified by Linear Mixed-Effects Models

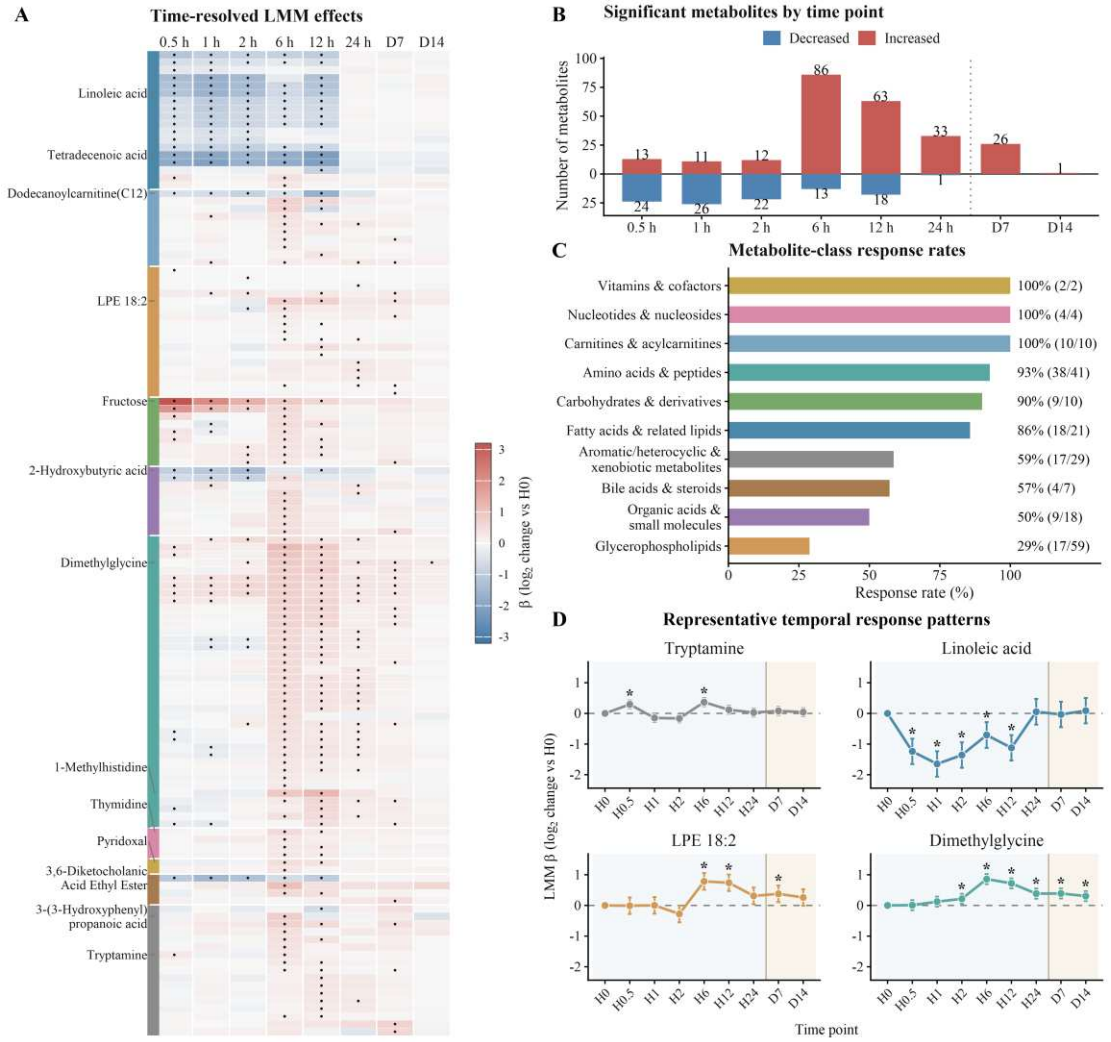

Fig. 3 Time-dependent metabolic responses revealed by linear mixed-effects models

(A) Heatmap of LMM β estimates for 128 metabolites with q<0.05 at one or more planned time points. Colors show $\log_2$ effects relative to H0 without row Z standardization; black dots indicate significant time-point contrasts. (B) Numbers of metabolites significantly increased and decreased at each time point. (C) Descriptive response rates and numbers responsive/total for the unified classes, not an enrichment analysis; class colors on the left match those in A. (D) β estimates and pointwise 95% CIs for four representative molecules, with asterisks indicating significant time points; all four plots share a y-axis. Significance refers to q<0.05 after joint BH-FDR correction of all 1,608 planned contrasts. The 95% CIs were not adjusted for multiple comparisons. Background bands distinguish baseline and the initial-intake observation window (H0–H24) from next-morning fasting time points after continued supplementation (D7 and D14); time points are equally spaced.

In the linear mixed-effects models, 155 of 201 metabolites (77.1%) had an overall time effect meeting q<0.05 after BH-FDR correction, and 128 (63.7%) changed significantly from H0 at one or more planned time points. The 201 metabolites and eight planned time points generated 1,608 contrasts, of which 349 (21.7%) met q<0.05 after joint BH-FDR correction (Fig. 3A; Supplementary Tables S2–S3). The direction

and time of the largest effect differed among these metabolites, indicating that the overall response comprised multiple temporal patterns. All 201 models converged; 15 had singular random-intercept fits, and residuals in some models showed tail deviations. After leave-one-participant-out refitting and reapplication of BH-FDR correction to the planned contrasts, the originally significant D14 contrast for dimethylglycine and contrasts for three linoleic acid-related molecules remained significant; some contrasts close to q=0.05 were more sensitive to participant composition.

The number of significantly changed metabolites peaked at H6–H12 (Fig. 3B). At H0.5, H1, and H2, 37, 37, and 34 metabolites, respectively, changed significantly, predominantly decreasing. This number rose to 99 at H6 (86 increased and 13 decreased), and 81 remained significant at H12 (63 increased and 18 decreased). The numbers declined to 34 and 26 at H24 and D7, respectively, mainly showing increases. At D14, only dimethylglycine was significantly higher than H0. Because H6 and H12 blood samples were collected after lunch and dinner, respectively, these broad responses must be interpreted in the context of meals and cannot be attributed solely to beetroot powder intake.

Descriptive response proportions across metabolite classes ranged from 28.8% to 100% (Fig. 3C). Carnitines and acylcarnitines, nucleotides and nucleosides, and vitamins and cofactors each had a 100% response proportion, but these classes contained only 10, 4, and 2 metabolites, respectively. Response proportions for amino acids and peptides, carbohydrates and their derivatives, and fatty acids and related lipids were 38/41 (92.7%), 9/10 (90.0%), and 18/21 (85.7%), respectively. Glycerophospholipids had the lowest proportion, 17/59 (28.8%). These proportions describe the response composition within the analytical panel and are not enrichment results.

Four representative metabolites showed different temporal trajectories (Fig. 3D). Tryptamine increased transiently at H0.5 and H6, with FCs of 1.23 (95% CI: 1.12–1.34, $q<0.001$) and 1.29 (95% CI: 1.18–1.41, $q<0.001$), respectively. Linoleic acid decreased throughout H0.5–H12, with the largest decrease at H1 (FC=0.32, 95% CI: 0.24–0.43, $q<0.001$), and was no longer significant at H24. LPE 18:2 increased at H6 and H12 and was again significantly elevated at D7 [FC=1.30 (95% CI: 1.08–1.57), $q=0.032$]. Dimethylglycine increased significantly from H2 onward, reaching its largest estimated effect at H6 [FC=1.81 (95% CI: 1.62–2.03), $q<0.001$], and remained significantly higher than H0 at D14 [FC = 1.24 (95% CI: 1.10–1.38), $q = 0.0021$].

3.4 Shared and Time-Specific Metabolic Responses

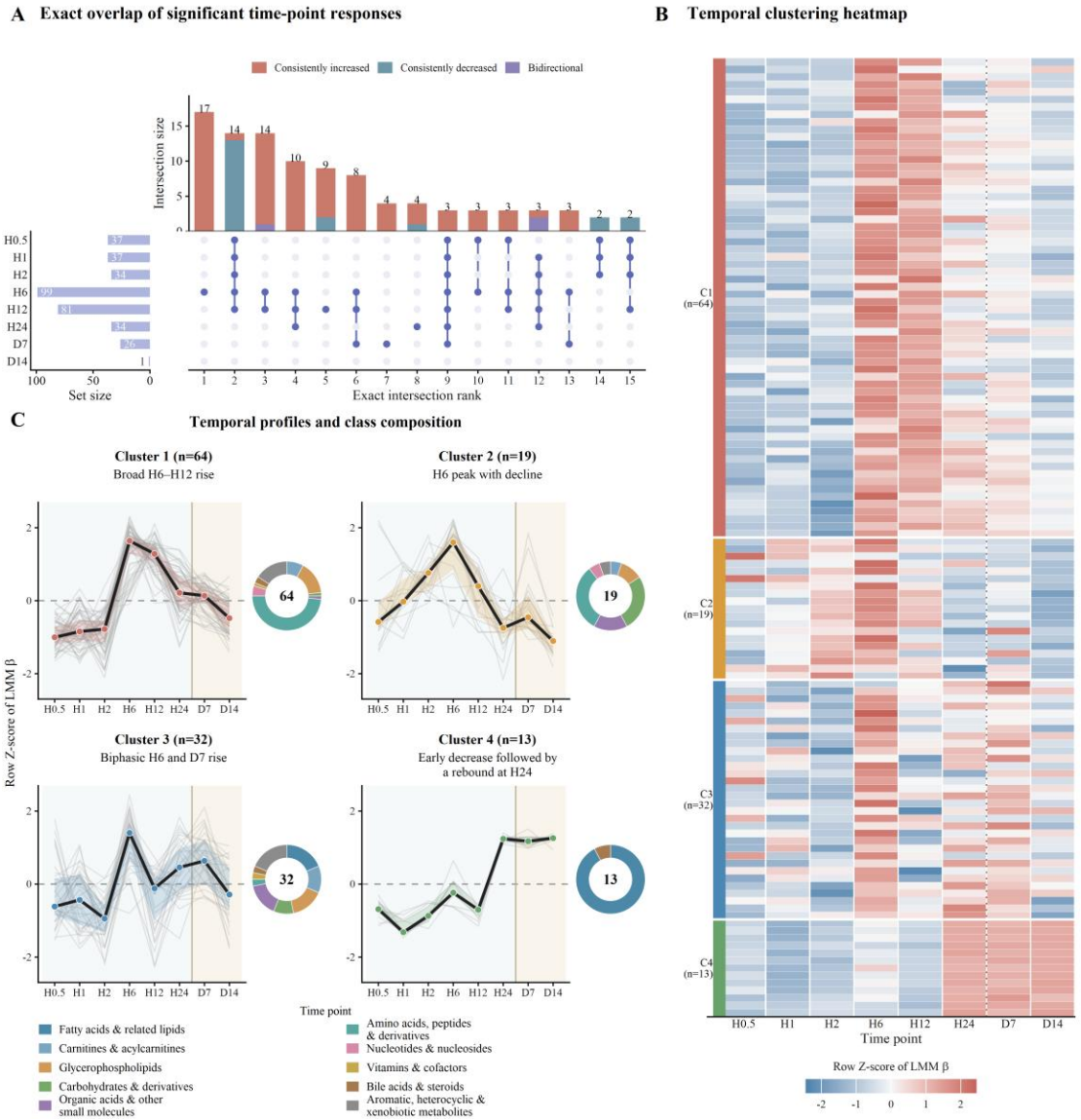

Fig. 4 Temporal overlap, clustering patterns, and metabolite-class composition of significant metabolic responses

(A) The 15 largest exact intersections of significant time points, covering 99/128 responsive metabolites. Bars above show the number of metabolites in each exact intersection, while bars at left show the total number significant at each time point. Dots and connecting lines indicate sets significant only at the displayed combination of time points; bar colors distinguish consistent increases, consistent decreases, and bidirectional changes. (B) Clustered heatmap of within-metabolite row-Z-standardized LMM β estimates for 128 responsive metabolites. (C) Gray lines show individual metabolite trajectories; black lines and colored points show within-cluster medians, and colored bands show interquartile ranges. Donut charts show class composition, with the central number indicating the number of metabolites in each cluster; class colors match Fig. 3. Significance denotes $q<0.05$ for contrasts with H0 after joint BH-FDR correction across all 1,608 planned contrasts. Dashed lines and background bands separate H0.5–H24 from D7–D14; time points are equally spaced. A positive Z score indicates an effect above that metabolite's mean effect across time points, not an increase relative to H0. Cluster membership also does not imply significance at every time point.

Exact-intersection analysis of the significant time points for the 128 responsive metabolites showed that the largest intersection comprised 17 metabolites significant only at H6, all of which increased (Fig. 4A). Another 14 were significant only at H0.5, H1, H2, H6, and H12; 13 decreased consistently and one increased consistently. Fourteen were significant only at H6 and H12; 13 increased consistently and one changed in opposite directions at the two time points. Ten metabolites significant only at H6, H12, and H24 and eight significant only at H6, H12, and D7 all increased consistently.

Four metabolites reached the significance threshold only at D7, all showing increases. At D14, only dimethylglycine (DMG) remained significantly elevated. The 15 largest exact intersections shown in Fig. 4A covered 99/128 responsive metabolites (77.3%; complete results are provided in Supplementary Table S4). Here, "time-specific" refers only to the combination of significant time points under the specified adjusted threshold and does not imply no change at other time points.

3.5 Clustering of Metabolite Temporal Patterns and Class Composition

Based on within-metabolite row-Z-standardized LMM β estimates for the 128 responsive metabolites at the eight nonbaseline time points, four temporal response clusters were identified, containing 64, 19, 32, and 13 metabolites, respectively (Fig. 4B–C; Supplementary Table S5).

Cluster 1 contained 64 metabolites (50.0%). Its standardized median trajectory was relatively low at H0.5–H2, rose to relatively high levels at H6–H12, and then declined. Amino acids, peptides, and their derivatives predominated, accounting for 48.4% (31/64). Cluster 2 contained 19 metabolites (14.8%); its standardized median trajectory rose gradually from H0.5 to H6, reached a relative peak at H6, and then declined. It mainly included amino acids, peptides, and their derivatives (6/19) and carbohydrates and their derivatives (5/19).

Cluster 3 contained 32 metabolites (25.0%). Its standardized median trajectory showed a relative trough at H2, rose at H6, declined at H12, rose again at H24–D7, and declined by D14; its class composition was relatively dispersed. Cluster 4 contained 13 metabolites (10.2%), of which 12 were fatty acids and related lipids (92.3%). Based on the LMM β estimates before row standardization, this cluster showed an early decrease followed by a rebound at H24, with effects close to zero at D7 and D14.

Row Z scores were used only to compare trajectory shapes within each metabolite; they cannot establish the direction of change relative to H0 or statistical significance. Complete cluster membership and effect estimates, along with diagnostics for choosing the number of clusters, are provided in Supplementary Table S5.

3.6 Metabolite-Class and Human Metabolic Pathway Characteristics of Temporal Response Clusters

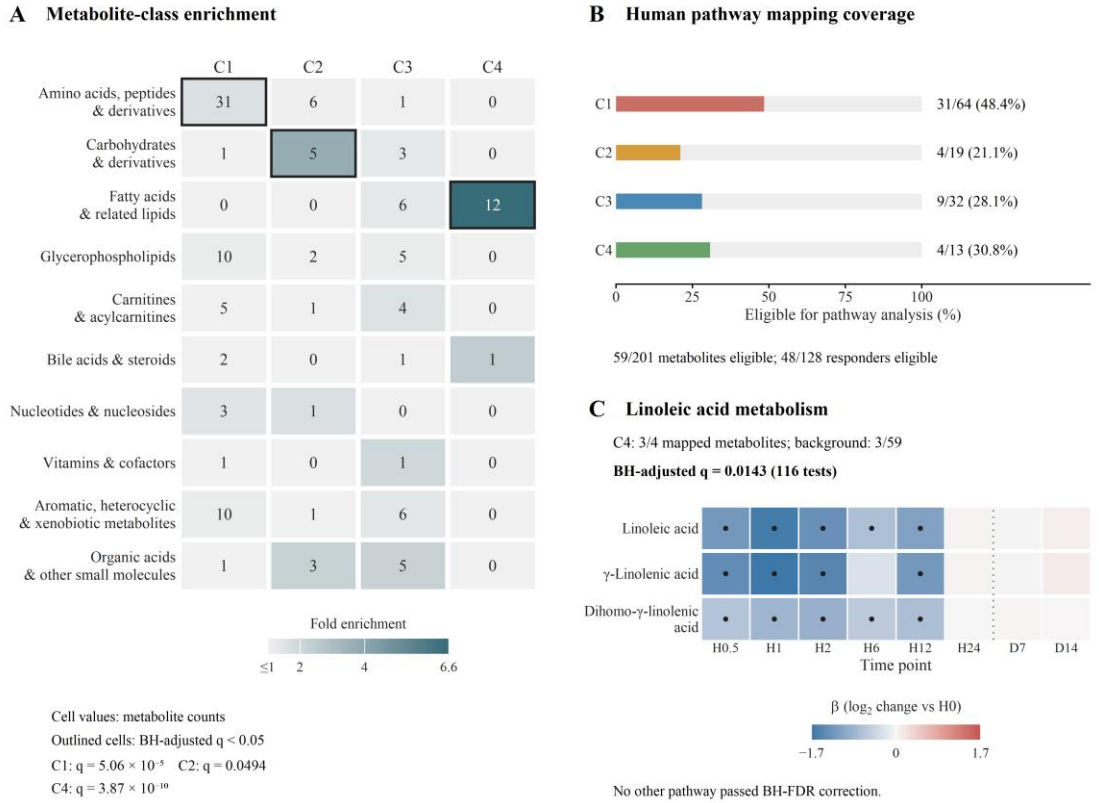

Fig. 5 Metabolite-class enrichment, human pathway mapping coverage, and linoleic acid metabolism features of temporal response clusters

(A) Class over-representation analysis for the four temporal response clusters. Numbers in cells indicate the number of metabolite hits; color indicates the ratio of the within-cluster proportion to the background proportion. Black borders indicate q<0.05 after joint BH-FDR correction of 40 tests across four clusters × 10 classes, using the 128 responsive metabolites as the background. (B) The number and proportion of metabolites in each cluster eligible for human KEGG pathway analysis. (C) LMM β estimates relative to H0 for the three metabolites in Cluster 4 that mapped to linoleic acid metabolism, without row Z standardization. The pathway q value comes from joint BH-FDR correction of 116 tests across four clusters × 29 pathways, with 59 mappable metabolites as the background; black dots in the heatmap indicate time-point contrasts with q<0.05 after joint correction of all 1,608 planned contrasts. The dashed line separates H0.5–H24 from D7–D14.

Using the 128 responsive metabolites as the background, BH-FDR correction was applied jointly to the 40 class over-representation tests formed by four temporal response clusters and 10 unified classes. Cluster 1 was enriched for amino acids, peptides, and their derivatives (31/64; odds ratio [OR]=7.65, $q=5.06\times10^{-5}$), Cluster 2 for carbohydrates and their derivatives (5/19; OR=9.38, q=0.0494), and Cluster 4 for fatty acids and related lipids (12/13; OR=218.00, $q=3.87\times10^{-10}$). No significant class enrichment was detected for Cluster 3 (Fig. 5A). Sensitivity analysis using all 201 retained metabolites as the background preserved these three findings (Supplementary Table S6).

Fifty-nine metabolites were included in the primary background for human KEGG pathway analysis, including 48 responsive metabolites. In Clusters 1–4, respectively, 31/64, 4/19, 9/32, and 4/13 members were eligible for pathway analysis (Fig. 5B). After joint correction of the 116 tests formed by four clusters and 29 pathways, only linoleic acid metabolism in Cluster 4 was significantly enriched (q=0.0143). Of the four mappable members of this cluster, linoleic acid, γ-linolenic acid, and dihomo-γ-linolenic acid mapped to this pathway. All three had negative LMM β estimates at H0.5–H12, with effects approaching zero at H24 and later time points (Fig. 5C); a negative β does not indicate significance at every time point. This pathway remained significant in sensitivity analyses using backgrounds of 48 responsive and mappable metabolites and 53 strictly mapped metabolites (Supplementary Table S7). Mapping coverage in pathway analysis was limited, and the class and pathway results involved overlapping molecules; they therefore cannot be regarded as independent mechanistic evidence.

3.7 Temporal Response Characteristics of Glycerophospholipid Subclasses and Molecular Species

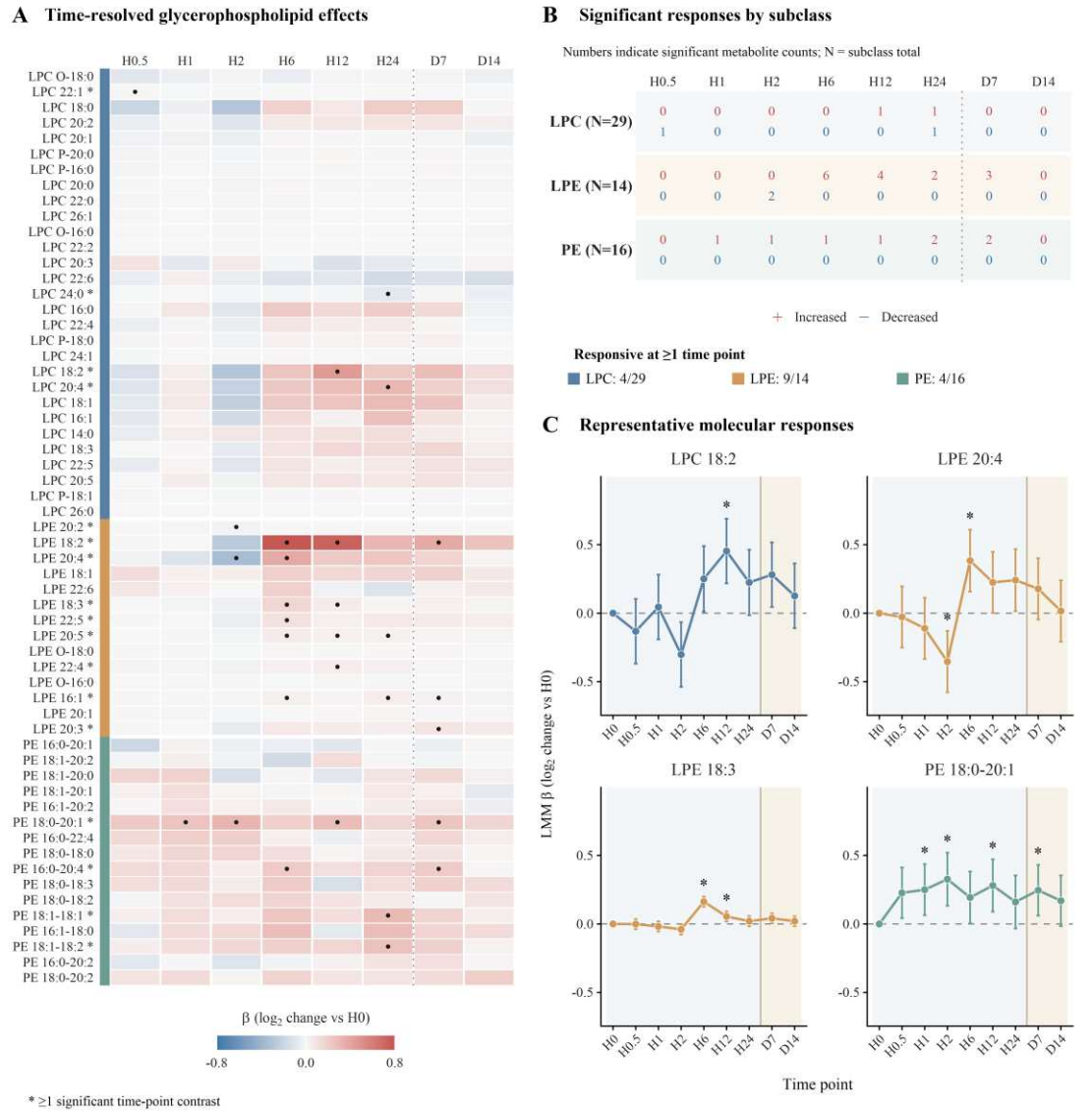

Fig. 6 Time-dependent responses of glycerophospholipid subclasses and molecular species
(A) LMM β estimates relative to H0 for all 59 retained glycerophospholipids, grouped into LPC, LPE, and PE blocks and without row Z standardization. An asterisk after a name indicates significance at one or more time points, and a black dot in the heatmap indicates significance at that specific time point. (B) Numbers of molecular species significantly increased or decreased in each subclass at each time point; N is the subclass denominator. These are descriptive summaries only, and counts across time points cannot be summed to obtain the number of distinct species. The numbers below show distinct species significant at one or more time points/total in the subclass. (C) β estimates and pointwise 95% CIs for four representative molecular species on a common y-axis; asterisks indicate significant time points. Significance refers to $q<0.05$ after joint BH-FDR correction of all 1,608 planned contrasts; the 95% CIs were not adjusted for multiple comparisons. LPC, LPE, and PE denote lysophosphatidylcholine, lysophosphatidylethanolamine, and phosphatidylethanolamine, respectively.

Because human KEGG pathway mapping does not adequately capture changes in specific glycerophospholipid molecular species, a further descriptive analysis was

conducted for all 59 retained glycerophospholipids: 29 lysophosphatidylcholines (LPCs), 14 lysophosphatidylethanolamines (LPEs), and 16 phosphatidylethanolamines (PEs). Seventeen changed significantly from H0 at one or more time points: 4/29 LPCs (13.8%), 9/14 LPEs (64.3%), and 4/16 PEs (25.0%; Fig. 6A–B). Significant LPE increases occurred mainly at H6 and H12, involving six and four species, respectively; two and three species were significantly increased at H24 and D7, respectively, while two decreased at H2. LPC responses were more scattered, and all significant PE time-point contrasts were increases. No glycerophospholipid molecular species changed significantly at D14.

Representative species showed different response directions and timing (Fig. 6C): LPC 18:2 increased significantly only at H12; LPE 20:4 decreased at H2 and increased at H6; LPE 18:3 increased at H6 and H12; and PE 18:0–20:1 increased at H1, H2, H12, and D7. LPE had the highest response proportion among the three subclasses, but these proportions are descriptive only. No between-subclass difference test was performed, and changes in a few molecular species cannot be generalized to a uniform response of all glycerophospholipids. Time-point effects for all glycerophospholipids and the post hoc selection rules for the four representative species are provided in Supplementary Table S8.

3.8 Temporal Responses of Betaine-Related and Other Candidate Metabolic Features

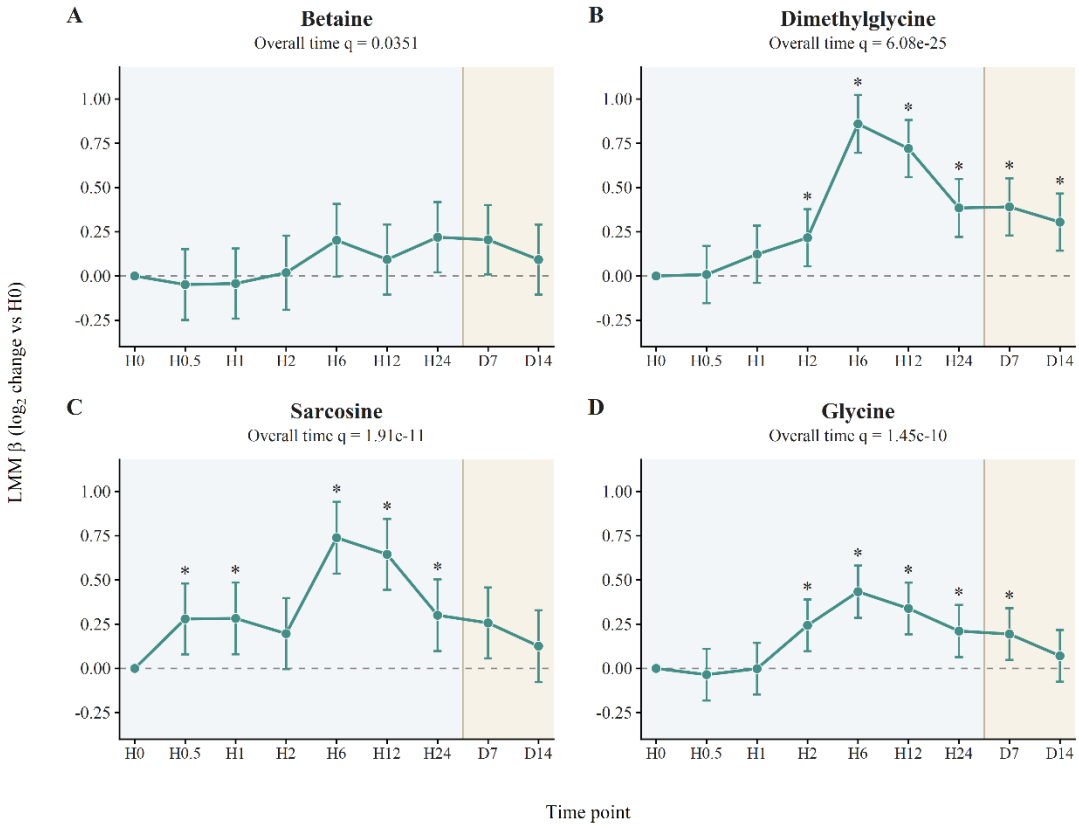

Fig. 7 Temporal responses of candidate betaine-related metabolites

(A–D) LMM effects β (on the $\log_2$ concentration scale) and pointwise 95% CIs relative to H0 for

betaine, dimethylglycine, sarcosine, and glycine. The four panels share a y-axis; H0 is set to zero effect, and gray dashed lines indicate β=0. The overall time-effect q values shown in each panel were obtained after BH-FDR correction across all 201 overall time-effect tests; asterisks indicate time points with q<0.05 after joint correction of all 1,608 planned contrasts. The 95% CIs were not adjusted for multiple comparisons. Dashed lines separate H0.5–H24 from D7–D14; time points are equally spaced and do not represent actual time intervals.

To supplement the overall and module-level results, temporal responses of betaine and related candidate metabolites were further described (Fig. 7). This presentation is based on the preceding LMM results and does not constitute a new pathway test. The overall time effect for betaine was statistically significant (q=0.0351), but none of its eight planned contrasts with H0 survived joint correction (Fig. 7A). Dimethylglycine was significantly elevated at H2, H6, H12, H24, D7, and D14, with the largest estimated effect at H6 [FC=1.814, 95% CI: 1.620–2.032]. It remained significantly higher than H0 at D14 [FC = 1.24, 95% CI: 1.10–1.38, q = 0.0021] and was the only significantly changed metabolite at that time point (Fig. 7B). Sarcosine increased significantly at H0.5, H1, H6, H12, and H24, but not at D7 or D14 (Fig. 7C). Glycine increased significantly at H2, H6, H12, H24, and D7, but not at D14 (Fig. 7D). The response time courses of the four metabolites were not identical; complete effect estimates are provided in Supplementary Table S9.

As a secondary exploration, citrulline decreased significantly at H0.5 and H1 and increased significantly at H12 and D7; ornithine increased significantly at multiple time points from H6 through D7; and homoarginine increased significantly at H6, H12, and H24. None of the three reached significance at D14 (Supplementary Table S9). This study did not directly measure L-arginine, nitrate, nitrite, or nitric oxide and therefore cannot be used to infer increased nitric oxide production.

4 Discussion

By combining dense sampling after the initial intake with next-morning fasting measurements after continued supplementation, this study observed widespread and temporally heterogeneous changes in plasma metabolites during beetroot powder supplementation. Of the 201 metabolites analyzed, 128 met the adjusted significance criterion relative to the initial baseline at one or more planned time points. The breadth of the response was greatest at H6–H12 and then narrowed; by D14, only dimethylglycine (DMG) remained significantly elevated. Fatty acid-related changes occurred mainly early after the initial intake, DMG still differed at later fasting time points, and glycerophospholipids showed molecular-species heterogeneity. These findings indicate that dynamic responses after the initial intake and fasting differences after continued supplementation provide complementary information, but they cannot yet all be attributed to an independent effect of beetroot powder.

Dense sampling helps identify response patterns that a single time point cannot reflect. The predominantly decreasing changes at H0.5–H2, predominantly increasing changes at H6–H12, and four distinct trajectories show that screening at a fixed time

point may capture only part of the full response process. Human studies of beetroot juice have shown dose- and time-dependent nitrate-related markers, while a continued supplementation study suggested that measurements in the fasting state and after intake on the same day have different implications (5, 6). A standardized-breakfast study also found differing time courses for amino acids and one-carbon metabolites (7). Thus, the greatest response breadth at H6–H12 is an observation within this study's sampling schedule and analytical panel; it does not mean that the true physiological peaks of all metabolites occurred during this period. All 26 metabolites significant at D7 increased, and most were also significant at other time points. For the few that met the adjusted threshold only at D7, their temporal characteristics must still be judged in light of effect sizes and estimation precision at adjacent time points.

Meal provision and time of day are important for interpreting these trajectories. H0.5 and H1 blood samples were collected before breakfast, so changes already present at these time points cannot be directly explained by the breakfast provided afterward. H2 followed breakfast, while H6 and H12 followed lunch and dinner, respectively. Their broad responses occurred under the combined conditions of beetroot powder intake, standardized meals, and the passage of time during the day. A human meal-challenge study observed postprandial increases in amino acids and sugars and decreases in some fatty acids [18], and a controlled-schedule study showed that circulating metabolites are affected by sleep–wake and feeding schedules [19]. A light-meal intervention can also alter one-carbon metabolites such as betaine, DMG, and sarcosine [20]. The amino acid and carbohydrate responses in Clusters 1 and 2 are compatible with postprandial changes, but their origins remain uncertain. Standardized meals improved comparability among participants but cannot substitute for a concurrent control. Fasting measurements at H24, D7, and D14 reduced differences in immediate feeding state, although earlier diet and fasting duration could still affect them.

Betaine-related molecules form a group of candidate features that merit priority for validation in this study. Betaine had a significant overall time effect, but no individual planned contrast survived joint correction; DMG, in contrast, increased at multiple time points beginning at H2 and still differed from the initial baseline at D14. The overall test and single-time-point contrasts address different questions and have different correction scopes, so these results are not contradictory. Jurga et al. observed that plasma betaine after beetroot juice intake reached its highest level among the designated sampling times at 1 h [4], and human studies directly administering betaine have also reported increased circulating DMG [21, 22]. These findings support the biological plausibility of the DMG response observed here. Differences between the single-time-point betaine results and earlier studies may involve product form, actual dose, population, sampling conditions, and the scope of multiple testing. Clifford et al.'s study of beetroot product composition and plasma detection further shows that product content does not directly represent circulating exposure [3]. Because the betaine

content of this batch of powder was not measured, the direct link between DMG and product intake remains to be verified.

Sarcosine and glycine add to these candidate features, but their significant time points did not fully coincide with those of DMG, and the entire group of molecules was not significantly elevated in parallel at D14. In a placebo-controlled randomized crossover trial, Nieman et al. observed increases in plasma betaine, DMG, and sarcosine after supplementation with pure betaine and reported a difference in cycling performance under that trial's conditions [23]. That study provides a basis for exercise-nutrition research on these molecules, but its intervention differed from the present study's, and simultaneous changes in metabolism and exercise performance do not establish a causal relationship between them. Together with the findings of the light-meal intervention [20], changes in these molecular concentrations may be influenced by both nutrient intake and endogenous metabolic regulation. Plasma concentrations are also affected by tissue distribution and clearance. This study therefore supports proposing betaine-related candidate metabolic features, while their conversion rates and functional significance require direct evidence.

Cluster 4 showed a relatively coherent fatty acid temporal pattern. Twelve of its 13 members were fatty acids and related lipids. Linoleic acid, γ-linolenic acid, and dihomo-γ-linolenic acid all had negative LMM effects at H0.5–H12, approaching zero at H24 and later time points. Linoleic acid metabolism was also the only human KEGG pathway that survived correction in this study. Significance persisted under different background definitions, supporting some robustness of the enrichment result. However, class membership, pathway membership, and member trajectories depend on overlapping molecules and cannot be regarded as independent mechanistic validation. Postprandial fatty acid changes also depend on the specific molecule, lipid fraction, and meal composition. Shokry et al. observed an early postprandial decline in total nonesterified fatty acids, whereas nonesterified linoleic acid within that pool increased earlier, and phospholipid fatty acids showed little overall change [24]. That finding, together with the negative effects already present before breakfast in this study, indicates that the entire module cannot simply be attributed to subsequent meals. The available evidence supports a consistent early fatty acid response, while its relationship to tissue uptake, fatty acid oxidation, and other metabolic processes remains undetermined.

The glycerophospholipid results show that broad class-level summaries may obscure molecular-species differences. Of 59 retained species, 17 changed significantly at one or more time points. The descriptive response proportion for LPE was relatively high, with increases concentrated mainly at H6–H12, whereas LPC and PE responses were limited to some species and time points. A human lipid-challenge study observed postprandial responses in specific LPE and PE species [25], and a plasma lipid time-series study showed substantial variation in within-day changes and between

individuals across species [26]. These studies support analyzing temporal trajectories at the molecular-species level and interpreting their sources cautiously in a single-group study. For lipid species with limited KEGG coverage, subclass composition and temporal trajectories can supplement pathway analysis. However, no formal between-subclass difference test was performed here, and links between concentration changes and membrane lipid turnover, lipoprotein transport, or related enzyme activities require further measurement.

The phase-specific responses of citrulline, ornithine, and homoarginine provide exploratory information on related amino acid metabolism. Previous human beetroot studies established evidence for nitrate-related responses by directly measuring nitrate, nitrite, and physiological endpoints (1, 5). The present metabolomics analysis did not directly measure L-arginine, nitrate, nitrite, or nitric oxide production, and the significant periods for these three molecules were not identical. They may therefore be candidate targets for subsequent measurement but do not yet provide direct evidence of enhancement of the nitrate–nitrite–nitric oxide pathway.

Strengths of this study include dense longitudinal sampling in the same cohort, clearly specified meal and sampling schedules, quantitative quality control, and joint multiple-testing correction across all planned time-point contrasts. Combining complete molecular effects with clustering, class, and pathway results also extended observation beyond a few preselected metabolites. The main limitation is the single-group design: supplement exposure, meals, and the passage of time occurred together, precluding estimation of the net effect of beetroot powder relative to no supplementation. This batch of product lacked measured information on components such as betaine, and D7 and D14 each included only one fasting sample, so maintenance of the same level between those two samples cannot be demonstrated. The study population of 24 healthy young men and the coverage of the targeted panel and KEGG mapping also limit generalizability and interpretation. The absence of a significant contrast for metabolites other than DMG at D14 does not imply their equivalence to baseline. Earlier metabolomics studies observed beetroot supplementation-related changes in serum after a marathon and in urine after exercise testing in fencers (8, 9). Their exercise loads, sample types, and sampling schedules differed from those here, and metabolic differences and functional improvement also require separate evaluation.

Future studies should measure key product constituents and their circulating exposure in randomized controlled designs with consistent meal, sampling, and analytical conditions, and should prespecify validation endpoints. Early and H6–H12 sampling should be retained after initial intake, while repeated standardized next-morning fasting samples are needed during continued supplementation. DMG and related one-carbon metabolites, linoleic acid-related fatty acids, and representative LPE species may be prioritized. If exercise capacity or the nitrate–nitric oxide pathway is examined further, corresponding functional and biochemical markers should be

measured simultaneously. This study identified plasma metabolic responses with distinct temporal features; the later fasting difference in DMG and early fatty acid changes offer relatively clear candidate leads, but their origins, specificity, and functional significance remain to be determined in controlled studies.

5 Conclusions

This study showed temporal and molecular heterogeneity in plasma metabolic responses during beetroot powder supplementation: widespread changes followed initial intake, whereas next-morning fasting differences after continued supplementation were relatively limited. The early decreases in some fatty acid-related molecules and increases in dimethylglycine at later fasting time points provide a basis for selecting candidate molecules and sampling times in controlled studies. Because a concurrent control was absent and relevant constituents of this product batch were not measured, these changes cannot yet be attributed independently to beetroot powder, nor can functional effects be inferred from them.

Supplementary Materials

The supplementary tables are provided in an accompanying Excel workbook. Table S1: Metabolite annotations and eligibility for human KEGG pathway analysis; Table S2: Overall time effects from linear mixed-effects models, valid observation counts by time point, and reasons for missing values; Table S3: Planned time-point contrasts against H0 for all analyzed metabolites; Table S4: Significant time-point overlap and response directions; Table S5: Time-response cluster membership, effect trajectories, and cluster-number selection; Table S6: Metabolite class over-representation analysis and background sensitivity analysis; Table S7: Human KEGG pathway over-representation analysis and sensitivity analyses; Table S8: Glycerophospholipid time-point contrasts and representative metabolite selection; Table S9: Overall time effects and planned time-point contrasts for candidate metabolites.

Acknowledgements

The authors thank the students of the Capital University of Physical Education and Sports who participated in this study.

Funding

This research was supported by the National Key Research and Development Program of China (project nos. 2018YFF0300603 and 2018YFF0300902), the Science and Technology Enhancement Project of Capital University of Physical Education and Sports (project no. 155226001/003), and the Sports Nutrition Center, National Institute of Sports Medicine, through the commissioned research project “Metabolic Kinetic Analysis of Red Beetroot Powder” (project no. 153225058). The commissioned project was administered by Capital University of Physical Education and Sports.

Author Contributions

Conceptualization, W.G., Z.H., H.W., and N.A.; methodology, W.G., Z.H., H.W., and N.A.; investigation, W.G. and T.L.; data curation, Z.H.; formal analysis, Z.H.; writing—original draft preparation, W.G. and Z.H.; writing—review and editing, H.W. and N.A.; supervision, H.W. and N.A. All authors have read and agreed to the published version of the manuscript.

Conflicts of Interest

The authors declare that they have no known competing financial interests or personal relationships that could have appeared to influence the work reported in this paper.

Data Availability Statement

The data that support the findings of this study are available from the corresponding authors upon reasonable request.

Ethics approval and consent to participate

This study was approved by the Ethics Committee of Capital University of Physical Education and Sports (approval no. 2025A162) and was conducted in accordance with the Declaration of Helsinki. All participants provided written informed consent before participation.

Declaration of generative AI and AI-assisted technologies in the writing process

During the preparation of this work, the authors used ChatGPT (OpenAI) to assist with English translation and language editing.

References

1. Webb, A.J.; Patel, N.; Loukogeorgakis, S.; Okorie, M.; Aboud, Z.; Misra, S.; Rashid, R.; Miall, P.; Deanfield, J.; Benjamin, N.; MacAllister, R.; Hobbs, A.J.; Ahluwalia, A. Acute blood pressure lowering, vasoprotective, and antiplatelet properties of dietary nitrate via bioconversion to nitrite. *Hypertension* **2008**, *51*, 784-790.
2. Larsen, F.J.; Schiffer, T.A.; Borniquel, S.; Sahlin, K.; Ekblom, B.; Lundberg, J.O.; Weitzberg, E. Dietary inorganic nitrate improves mitochondrial efficiency in humans. *Cell Metabolism* **2011**, *13*, 149-159.
3. Clifford, T.; Constantinou, C.M.; Keane, K.M.; West, D.J.; Howatson, G.; Stevenson, E.J. The plasma bioavailability of nitrate and betanin from Beta vulgaris rubra in humans. *European Journal of Nutrition* **2017**, *56*, 1245-1254.
4. Jurga, J.; Samborowska, E.; Zielinski, J.; Olek, R.A. Effects of Acute Beetroot Juice and Sodium Nitrate on Selected Blood Metabolites and Response to Transient Ischemia: A Crossover Randomized Clinical Trial. *The Journal of Nutrition* **2024**, *154*, 491-497.
5. Wylie, L.J.; Kelly, J.; Bailey, S.J.; Blackwell, J.R.; Skiba, P.F.; Winyard, P.G.; Jeukendrup, A.E.; Vanhatalo, A.; Jones, A.M. Beetroot juice and exercise: pharmacodynamic and dose-response relationships. *Journal of Applied Physiology* **2013**, *115*, 325-336.
6. Miller, G.D.; Collins, S.; Ives, J.; Williams, A.; Basu, S.; Kim-Shapiro, D.B.; Berry, M.J. Efficacy and Variability in Plasma Nitrite Levels during Long-Term Supplementation with Nitrate Containing Beetroot Juice. *Journal of Dietary Supplements* **2023**, *20*, 885-910.
7. Anfinsen, Å.M.; Johannesen, C.O.; Myklebust, V.H.; Rosendahl-Riise, H.; McCann, A.; Nygård, O.K.; Dierkes, J.; Lysne, V. Time-resolved concentrations of serum amino

acids, one-carbon metabolites and B-vitamin biomarkers during the postprandial and fasting state: the Postprandial Metabolism in Healthy Young Adults (PoMet) Study. *British Journal of Nutrition* **2024**, *131*, 786-800.

8. Kozlowska, L.; Mizera, O.; Mroz, A. An Untargeted Metabolomics Approach to Investigate the Metabolic Effect of Beetroot Juice Supplementation in Fencers—A Preliminary Study. *Metabolites* **2020**, *10*, 100.
9. Stander, Z.; Luies, L.; van Reenen, M.; Howatson, G.; Keane, K.M.; Clifford, T.; Stevenson, E.J.; Loots, D.T. Beetroot juice - a suitable post-marathon metabolic recovery supplement? *Journal of the International Society of Sports Nutrition* **2021**, *18*, 72.
10. Mrakic-Sposta, S.; Vezzoli, A.; Parenza, M.; Magno, M.; D'Angelo, G.; Nannipieri, F.; Battaglia, S.; Solfanelli, L.; Tacconi, E.; Dellanoce, C.; Montorsi, M.; Pratali, L. Effect of Beetroot Nitrate Supplementation on Nitric Oxide Pathways and Oxy-Inflammatory Biomarkers in Amateur Triathletes: A Randomized Cross-Over Pilot Study. *Nutrients* **2026**, *18*, 1215.
11. Kapil, V.; Haydar, S.M.A.; Pearl, V.; Lundberg, J.O.; Weitzberg, E.; Ahluwalia, A. Physiological role for nitrate-reducing oral bacteria in blood pressure control. *Free Radical Biology and Medicine* **2013**, *55*, 93-100.
12. MacLean, B.; Tomazela, D.M.; Shulman, N.; Chambers, M.; Finney, G.L.; Frewen, B.; Kern, R.; Tabb, D.L.; Liebler, D.C.; MacCoss, M.J. Skyline: an open source document editor for creating and analyzing targeted proteomics experiments. *Bioinformatics* **2010**, *26*, 966-968.
13. Kanehisa, M.; Furumichi, M.; Sato, Y.; Matsuura, Y.; Ishiguro-Watanabe, M. KEGG: biological systems database as a model of the real world. *Nucleic Acids Research* **2025**, *53*, D672-D677.
14. van den Berg, R.A.; Hoefsloot, H.C.J.; Westerhuis, J.A.; Smilde, A.K.; van der Werf, M.J. Centering, scaling, and transformations: improving the biological information content of metabolomics data. *BMC Genomics* **2006**, *7*, 142.
15. Bates, D.; Mächler, M.; Bolker, B.; Walker, S. Fitting Linear Mixed-Effects Models Using lme4. *Journal of Statistical Software* **2015**, *67*, 1-48.
16. Kuznetsova, A.; Brockhoff, P.B.; Christensen, R.H.B. lmerTest Package: Tests in Linear Mixed Effects Models. *Journal of Statistical Software* **2017**, *82*, 1-26.
17. Rousseeuw, P.J. Silhouettes: A graphical aid to the interpretation and validation of cluster analysis. *Journal of Computational and Applied Mathematics* **1987**, *20*, 53-65.
18. Karimpour, M.; Surowiec, I.; Wu, J.; Gouveia-Figueira, S.; Pinto, R.; Trygg, J.;

Zivkovic, A.M.; Nording, M.L. Postprandial metabolomics: A pilot mass spectrometry and NMR study of the human plasma metabolome in response to a challenge meal. *Analytica Chimica Acta* **2016**, *908*, 121-131.

19. Skene, D.J.; Skornyakov, E.; Chowdhury, N.R.; Gajula, R.P.; Middleton, B.; Satterfield, B.C.; Porter, K.I.; Van Dongen, H.P.A.; Gaddameedhi, S. Separation of circadian- and behavior-driven metabolite rhythms in humans provides a window on peripheral oscillators and metabolism. *Proceedings of the National Academy of Sciences* **2018**, *115*, 7825-7830.
20. Helland, A.; Bratlie, M.; Hagen, I.V.; Midttun, Ø.; Ulvik, A.; Mellgren, G.; Ueland, P.M.; Gudbrandsen, O.A. Consumption of a light meal affects serum concentrations of one-carbon metabolites and B-vitamins. A clinical intervention study. *British Journal of Nutrition* **2023**, *129*, 1350-1359.
21. Schwahn, B.C.; Hafner, D.; Hohlfeld, T.; Balkenhol, N.; Laryea, M.D.; Wendel, U. Pharmacokinetics of oral betaine in healthy subjects and patients with homocystinuria. *British Journal of Clinical Pharmacology* **2003**, *55*, 6-13.
22. Grizales, A.M.; Patti, M.-E.; Lin, A.P.; Beckman, J.A.; Sahni, V.A.; Cloutier, E.; Fowler, K.M.; Dreyfuss, J.M.; Pan, H.; Kozuka, C.; Lee, A.; Basu, R.; Pober, D.M.; Gerszten, R.E.; Goldfine, A.B. Metabolic Effects of Betaine: A Randomized Clinical Trial of Betaine Supplementation in Prediabetes. *The Journal of Clinical Endocrinology & Metabolism* **2018**, *103*, 3038-3049.
23. Nieman, D.C.; Sakaguchi, C.A.; Williams, J.C.; Lawson, J.; Lambirth, K.C. Betaine Supplementation Improves 60 km Cycling Time Trial Performance and One-Carbon Metabolism in Cyclists During Recovery. *Nutrients* **2025**, *17*, 2765.
24. Shokry, E.; Raab, R.; Kirchberg, F.F.; Hellmuth, C.; Klingler, M.; Demmelmair, H.; Koletzko, B.; Uhl, O. Prolonged monitoring of postprandial lipid metabolism after a western meal rich in linoleic acid and carbohydrates. *Applied Physiology, Nutrition, and Metabolism* **2019**, *44*, 1189-1198.
25. Morris, C.; O'Grada, C.M.; Ryan, M.F.; Gibney, M.J.; Roche, H.M.; Gibney, E.R.; Brennan, L. Modulation of the lipidomic profile due to a lipid challenge and fitness level: a postprandial study. *Lipids in Health and Disease* **2015**, *14*, 65.
26. Chua, E.C.-P.; Shui, G.; Lee, I.T.-G.; Lau, P.; Tan, L.-C.; Yeo, S.-C.; Lam, B.D.; Bulchand, S.; Summers, S.A.; Puvanendran, K.; Rozen, S.G.; Wenk, M.R.; Gooley, J.J. Extensive diversity in circadian regulation of plasma lipids and evidence for different circadian metabolic phenotypes in humans. *Proceedings of the National Academy of Sciences* **2013**, *110*, 14468-14473.